Heat Mass Transfer (2008) 44:1537–1547
DOI 10.1007/s00231-008-0387-3

ORIGINAL

A study of loop heat pipe with biporous wicks

C. C. Yeh · B. H. Liu · Y. M. Chen

Received: 8 October 2007 / Accepted: 26 February 2008 / Published online: 10 April 2008

Abstract The purpose of this study is to investigate the effects of various bimodal pore size distributions of biporous wicks for a loop heat pipe (LHP). The study was conducted following a statistical method using a two-level factorial plan involving three variables (particle size of pore former:74–88 and 125–149 μm Na_2CO_3, pore former content:20% by volume and 25% by volume, sintering temperature:700 and 750°C). Finally, the heat transport capability of the LHP between monoporous wicks and biporous wicks has been investigated. Experimental results show that, at the sink temperature of 10°C and the allowable evaporator temperature of 80°C, the heat transfer capacity of the better biporous wick achieved 200 W and the total thermal resistance was 0.31°C/W. The performance is enhanced about 60%, compared to a monoporous wick for 125 W and 0.53°C/W. Therefore, LHPs with biporous wicks are very attractive for high heat flux applications in the future.

List of symbols

R_{tot}	total thermal resistance °C/W
Q	heat load W
T_e	evaporator temperature °C
T_c	condenser temperature °C
K_w	permeability m^2
m_l	mass flow rate of the liquid kg/s
D_o	outer diameter of the wick sample m
D_i	inner diameter of the wick sample m
ΔP	pressure drop across the wick kg/m s^2
L_w	wick length m

Greek symbols

μ_l	liquid viscosity kg/m s
ρ_l	liquid density kg/m^3

Subscripts

e	evaporator
c	condenser
l	liquid
w	wick
o	outer
i	inner
tot	total

C. C. Yeh · B. H. Liu · Y. M. Chen (✉)
Department of Mechanical Engineering,
National Taiwan University,
Taipei 10764, Taiwan, ROC
e-mail: ymchen@ntu.edu.tw

C. C. Yeh
e-mail: D94522027@ntu.edu.tw

1 Introduction

The loop heat pipe (LHP) was first invented by Maidanik in the mid-1980s [1]. LHPs could achieve high heat transfer capacity, long transport distance and low thermal resistance. In addition, LHPs possess the advantages including simple structure, reliability, self-priming and active control. It is very suitable for electronic equipments that need dissipating great quantity of heat. In 1994 Wolf et al. [2] investigated the properties and the applicable potential about LHPs. They considered that LHPs combine the advantages for heat pipe and capillary pump loop (CPL). LHPs will become the highly efficient heat-transfer device. In view of the preceding reasons, the LHP is chosen to be the object of research in the study. The

design of wick structure parameters (effective pore radius, porosity, and permeability) in the evaporator would be the key impact on the performance of a LHP. Phase change can be generated to transport heat at the interface between liquid and vapor by the wick when heat is applied to the evaporator. On the other hand, there is the correlation between the capillary pressure and heat transport capability because the capillary pressure in the wick provides the required pressure to circulate the fluid in the system. Gerhart et al. [3] pointed out that the wick made of sintered metal with very fine pores (on the order of 1 μm) can be operated against gravity efficiently and possess higher heat transport capability. Although a wick with the small effective pore radius can generate the high capillary pressure, it can have a low permeability to reduce the working fluid across the wick. Therefore, the compromise between the effective pore radius and the permeability is necessary to achieve the better heat transport capability for the design of monoporous wicks.

In recent years, researchers have paid more attention to miniature LHPs for cooling of high-power electronic and optical components. With the increasing usage of miniature LHPs, the properties of a wick structure in the evaporator have become more critical. Especially at high heat flux rates, a monoporous wick is intolerant of boiling and the intensive liquid-vapor interactions influence the returning liquid flow, leading to dry-out in the wick structure.

In order to solve the limitation about the properties of a monoporous wick, Konev et al. [4] investigated boiling phenomenon in wick structures and pointed that a bidisperse wick enhances the boiling heat transfer to a greater extent than a monoporous wick. In addition, Rasor and Desplat [5] proposed that an analytical model has been derived for the temperature drops and heat flux limits for heat transfer through a biporous material called K-MAX, which is similar to a heat pipe. They noticed that the heat flux limits are exceedingly sensitive to the volume fractions of liquid and vapor phases in a biporous wick structure.

Afterwards, Rosenfeld and North [6] reported that a bidisperse wick takes advantage of the highly effective heat transfer intrinsic to liquid film evaporation. When higher heat load is applied to the bidisperse wick, the evaporating menisci area will be extensive. Until 1997, North et al. [7] first applied a bidisperse wick to a LHP evaporator. They pointed out that the bidisperse wick increases the thermal conductivity and the evaporating surface area in the region of highest heat flux, while providing a flow path for the vapor. However, there are no specifying descriptions of the procedure for making the bidisperse wick and the effect of the bidisperse wick parameters.

Sintered copper bidisperse wicks and distilled water were used for the experimental study by Chen et al. [8] in 2000. The results showed that the porous material has a highly effective two-phase heat sink, especially for bidisperse wicks which have a lower flow resistance than that of the monoporous wicks having the same pore diameter as the micro-pore diameter of the bidisperse wick. Then, Cao et al. [9] reported that an experiment has been carried out on evaporative heat transfer in rectangular bidisperse wick structures heated by a grooved block from the top. They investigated an optimal ratio of large and small pore diameters (400 μm/80 μm) for sintered copper bidisperse wicks. It gives both the highest heat transfer coefficient and the highest critical heat flux. However, the applications of the foregoing bidisperse wick parameter in heat pipes and LHPs have not yet been much explored.

In subsequent years numerous studies were carried out on the effectiveness of biporous wicks for heat pipes. In 2001 a biporous heat pipe was proposed to overcome heat transfer crisis in the evaporator by Wang and Catton [10]. Thermal analysis of a solid copper spreader, monoporous and biporous heat pipe modules were performed. Comparison of the results showed the heat transfer performance of the monoporous and biporous heat pipes are better than the solid copper spreader, and the biporous heat pipe has an advantage in the relatively high heat flux range for cooling electronic devices. Semenic and Catton [11] investigated the effect of biporous wick parameters such as wick thickness, powder size, and cluster size for a heat pipe, powder size especially. Review and summarize previous studies, it may enhance effectively the heat transport capability if there are the biporous wicks and wicks with inverted menisci in a LHP.

Although much work have been noted that biporous wicks can improve the heat transfer performance and enhance critical heat fluxes for heat pipes and pool boiling, there is very limited study on the effects of the biporous wicks for LHPs.

As reviewed and summarized previous studies, the purpose of this study was to investigate the effects of various bimodal pore size distributions of biporous wicks for a LHP. A statistical method was used to analyze the heat transfer capacity of biporous wicks and to find out the better bimodal pore size distribution for a biporous wick.

The article is structured as follows. The Sect. 1 introduces the principle of LHP operation and LHP geometric characteristics. The Sect. 2 describes the research method, including the fabrication, the design of experiments, and the measurement for the properties of biporous wicks. The Sect. 3 analyzes the resulting data and discusses the relationship between the pore size distributions and the heat transfer capacities of the wick structures. Finally, conclusions and suggestions are presented.

2 LHP principles

2.1 The principle of LHP operation

A LHP consists of five components: an evaporator, a compensation chamber, a condenser, a liquid line, and a vapor line. Only the evaporator section has a wick structure and other components are constructed by smooth tubes, as shown in Fig. 1.

The main purpose of a wick is to generate phase changes and the capillary pumping pressure required to circulate a working fluid, as shown in Fig. 2. When heat is applied to the evaporator, it is conducted into the working fluid at the surface of the wick structure. The working fluid is vaporized to generate the liquid-vapor interface in the wick. The evaporating menisci are inverted towards the wall being heated. This is called the principle of inverted menisci. The vapor is then easily escaped from the wick and is collected by vapor channels. Because the vapor in the vapor channels has the highest pressure in the system, it flows through the vapor line to the condenser. After being condensed, the working fluid will return to the evaporator through the liquid line. The liquid line can be extended to the evaporator core by the bayonet between the evaporator and the compensation chamber. The bayonet leads the liquid to the evaporator core before reaching the closed end. The wick structure is kept in the wet state by the liquid. The excess liquid returns to the compensation chamber, which is used to regulate the liquid inventory in the loop as well as to regulate the operation temperature. This completes the flow cycle in a LHP.

2.2 Loop heat pipe setup

The performance of a LHP depends on the design of the vapor channels and the wick. In order to differentiate the effects between vapor channels and wick parameters, the design of vapor channels was fixed to the evaporator in this study. The heat transport capability of the LHP was observed by only changing wick parameters. The LHP system designed for the monoporous wick was used to test the heat transport capability of the biporous wick. The geometric characteristics of the LHP are presented in Table 1.

The LHP system was built with stainless steels and the capillary evaporator had a wick made of sintered nickel. In this case, ammonia was used as the working fluid and the temperature ranges from -20 to $+$ 80°C. The environmental temperature was controlled from 19 to 22°C in most of the experiments. Here, the sink temperature was simulated by a water cooler which was controlled at 10°C. Heat load was applied to the evaporator through cartridge heaters attached to the copper saddle by a DC power supply (deviation of $\pm$ 0.5 W) and the heating surface area was 800 mm^2.

The capability of a LHP was usually evaluated by the indexes of the input heat load and the total thermal resistance. Therefore, it was necessary to record the heating power and the loop's temperature distribution through thermocouples during the test. The temperature data was collected by recorder and then transferred to the computer through a GPIB card. Twelve T-type thermocouples (deviation of $\pm$0.2°C) are installed throughout the loop heat pipe in Fig. 3.

The total thermal resistance would be obtained by the respective temperature of the evaporator and condenser, expressed as

$$R_{\text{tot}} = \frac{T_{\text{e}} - T_{\text{c}}}{Q} \tag{1}$$

Here, the uncertainty analysis of the total thermal resistance was estimated to be within $\pm$ 2.48%.

2.3 Research method

In general, the heat transport capability of a LHP is determined by the design of the wick structure, the

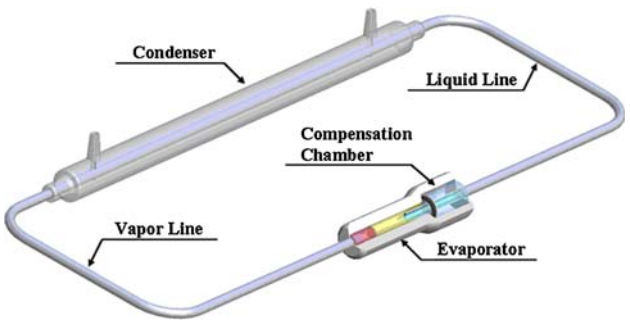

Fig. 1 Principal scheme of a LHP

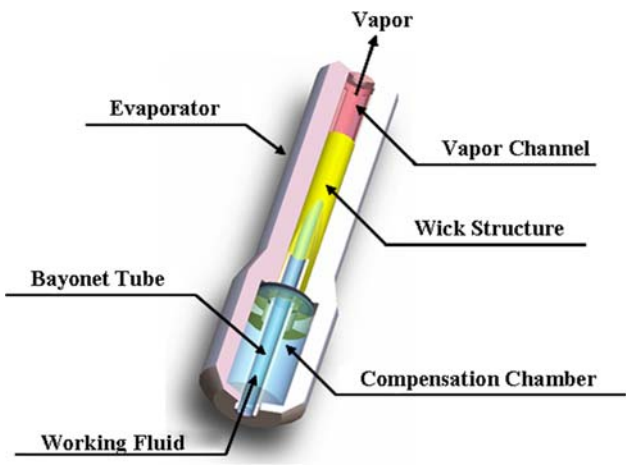

Fig. 2 Schematic diagram of the evaporator section

Table 1 LHP geometric characteristic

Capillary evaporator		Vapor line	
Total length (mm)	65	Outer diameter (mm)	6.4
Active length (mm)	40	Inner diameter (mm)	5
Outer/inner diameter (mm)	16/11	Length (mm)	470
Material	Stainless steel		
Number of vapor grooves	10		
Sintered nickel wick		Liquid line	
Pore radius (μm)	3–30	Outer diameter (mm)	6
Permeability (m^2)	10^{-11}–10^{-12}	Inner diameter (mm)	3
Outer/inner diameter (mm)	11/8	Length (mm)	583
Compensation chamber		Condenser	
Volume (cm^3)	53.4	Outer diameter (mm)	6.4
Outer/inner diameter (mm)	29/24	Inner diameter (mm)	5
Length (mm)	118	Length (mm)	800
Bayonet		Charge mass	
Outer diameter (mm)	5	Ammonia (g)	37
Inner diameter (mm)	3		
Length (mm)	129		

evaporator, and compensation chamber, in particular of the wick structure. It affects directly the whole heat transport capability of a LHP because the phase change occurs inside the wick. The potency of a LHP can be exhibited if the manufacturing technology of the wick structure is controlled. Following is an illustration of different types of the wick structures with bimodal pore size distributions, the manufacturing method, the experimental design, wick properties, and measurement methods in the research.

2.4 Different types of the wick structures with bimodal pore size distributions

In general, there are two different methods to manufacture wick structures with bimodal pore size distributions: consolidation of porous particles and creation of biporous materials. In the first type the clusters formed by porous particles contain small pores, whereas between them there are coarse large pores. The size and amount of small pores are determined by sintering metal powder and those of large pores are formed passively by the clusters.

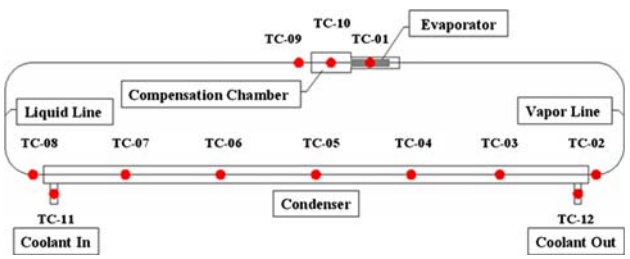

Fig. 3 Schematic of the LHP with location of thermocouples

For another type, small pores can be generated by sintering metal powder and larger pores can be formed by dissolving the pore formers. The size and amount of small pores are determined by sintering metal powder and those of large pores are controlled easily by the pore formers.

In order to control easily various bimodal pore size distributions in the biporous wicks, the second type was used to investigate the effects of various bimodal pore size distributions of biporous wicks for a LHP.

2.5 Fabrication of the biporous wick structure

In order to generate the wick with a bimodal pore size distribution, the manufacturing method is described as below. First of all, pore formers (Na_2CO_3) which had suitable particle sizes (74–88 and 125–149 μm) and content (20% by volume and 25% by volume) were mixed uniformly with filamentary nickel powder. A V-type mixer was used. Then, the mixing powder filled into the mold was sintered in the furnace. The smaller pore size distribution of the biporous wick could be generated by sintering the nickel powder; the larger pore size distribution of the biporous wick could be generated by dissolving the pore formers in water after the sintering process. On the other hand, pore formers were used to control the size and amount of larger pores in the wick. Finally, there were two different types of pore sizes in the wick at the same time. The appearance and structure of the biporous wick (Sample 7) can be observed in Figs. 4 and 5, respectively. Low-power SEM (250×) of the biporous wick obviously shows that two different types of pore sizes are existed in Fig. 5a.

Fig. 4 The appearance of the biporous wick

High-power SEM (2,000×) of the biporous wick presents that the smaller pore sizes are generated by sintering the nickel powder in Fig. 5b.

2.6 Design of experiments for biporous wicks

To search for the better bimodal pore size distribution of a biporous wick applied to a LHP, a statistical experimental design is used to increase the efficiency of these experiments and to make the results be objective rather than judgmental in nature.

Monoporous wicks and biporous wicks were made by the same nickel powder as a basic component. When sintered, the filamentary nickel powder with the particle size 3 μm can produce a narrow pore size distribution curve and a highly porous nickel structure. As observed in Table 2, three variables can be controlled during the fabrication of the biporous wicks.

The experimental design is that of three factors such as particle size of pore former (A), pore former content (B), and sintering Temperature (C), each run at two levels. This is a 2^3 factorial design. The variables A, B, and C are defined on a coded scale from −1 to +1 (the low and high levels of A, B, and C). Finally, the regression model could be represented by the terms of coded factors, where the former is calculated by Eqs. (2)–(4) below:

$$A_{\text{code}} = (A - 99.5\,\mu\text{m})/25.5\,\mu\text{m} \quad (2)$$

$$B_{\text{code}} = (B - 22.5\%)/2.5\% \quad (3)$$

$$C_{\text{code}} = (C - 725^{\circ}\text{C})/25^{\circ}\text{C}. \quad (4)$$

The heat transport capability of the LHP was observed by only changing wick parameters. The parameters of the two monoporous wicks and eight biporous wicks are listed in Table 3. Other properties, including porosity and permeability of the tested wicks are also listed in Table 3.

For the heat transport capability of the LHP, the temperature change in the evaporator body was measured by per 25 W and the heat load was increased from 25 to 200 W. In order to examine the whole of heat transfer capacity for the specific wick, the response variable measured was the aggregate value of evaporator temperature from 25 to 200 W. Finally, the experimental results identified and investigated by statistical analysis were used to develop a regression model. Then, the response surface plot generated by the regression model could be used to find a direction of potential improvement for a fabrication of biporous wick. This information would provide a practical interpretation of this experiment.

2.7 Wick properties

In general, there are three major properties of the wick that have to be considered, including effective capillary radius, wick permeability, and porosity. Optimum values of heat transport capability occur due to the influence of the

Table 2 The selected process variables and experimental deign levels used

Variables	Code	Unit	−1	+1
Particle size of pore former	A	μm	74–88	125–149
Pore former content	B	%	20	25
Sintering temperature	C	°C	700	750

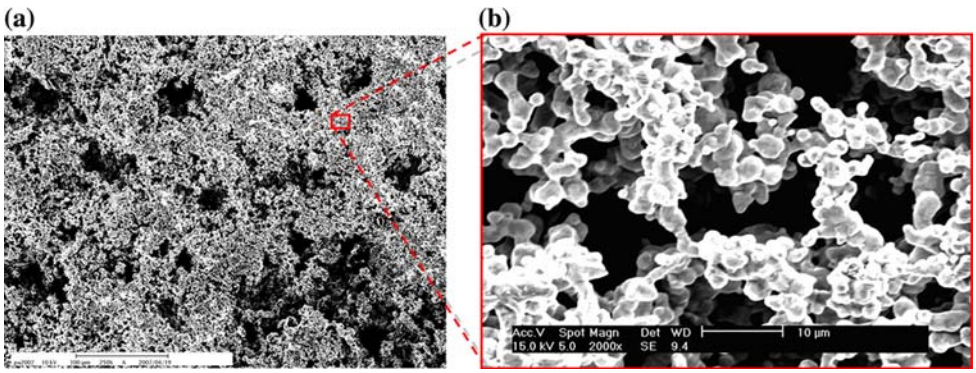

Fig. 5 The structure of the biporous wick **a** low-power SEM (250×) of the biporous wick, **b** high-power SEM (2,000×) of the biporous wick

Table 3 Properties of the wicks tested

Sample	Experimental design variables				Response							Porosity (%)	Permeability (10^{-12} m^2)
	Values				Evaporator temperature (°C)								
	NPS (μm)	A (μm)	B (%)	C (°C)	25 W	50 W	75 W	100 W	125 W	150 W	175 W	200 W	The aggregate value		
Biporous wick															
1	3	74–88	20	700	30.5	37.2	44.6	50.8	62.3	72.1	76.7	85.0	459.2	81.4	4.34
2	3	125–149	20	700	32.2	46.2	58.6	61.3	70.4	78.1	82.9	90.1	519.8	82.6	5.55
3	3	74–88	25	700	29.7	38.7	39.0	42.6	49.1	59.7	74.8	82.4	416.0	85.0	10.61
4	3	125–149	25	700	32.3	38.7	44.2	52.7	60.8	66.9	72.4	81.3	449.3	86.5	17.37
5	3	74–88	20	750	30.6	39.1	45.0	51.8	60.2	66.4	69.7	74.3	437.1	78.4	3.64
6	3	125–149	20	750	32.4	43.5	54.2	59.3	68.4	79.9	71.8	83.2	492.7	78.5	3.86
7	3	74–88	25	750	29.4	36.6	42.1	45.7	48.6	55.9	68.8	73.2	400.3	83.1	10.34
8	3	125–149	25	750	34.3	41.9	50.1	56.4	55.4	57.4	62.6	69.9	428.0	85.2	11.77
Monoporous wick															
9	3	–	–	700	–	49.9	65.8	81.0	97.9	114.7	139.3	164.4		71.9	0.90
10	3	–	–	600	–	44.8	59.7	68.1	75.8	86.3	99.7	117.1		75.6	1.42

NPS nickel powder size (μm), *A* particle size of pore former (μm), *B* pore former content (%), *C* sintering temperature (°C)

effective capillary radius and porosity on both capillary pressure and permeability values. According to the above-mentioned result, wick properties are necessary to measure. If the major properties of the wick are controlled, the heat transport capability can be enhanced obviously by the fine parameter of wick properties.

2.8 Measurement of the effective pore radius

The effective pore radius not only determines the capillary limit of a wick but also influences the heat transport capability of the LHP. Wang and Catton [12] noted that the average heat transfer coefficients increase with decreasing of pore sizes. For the design of a wick, reliable information about the pore size distribution of a wick is needed. This information allows us to compare wicks manufactured in different conditions and improve wick properties. In general, the effective pore radius of a wick can be measured by the bubble point method and the mercury intrusion porosimetry method.

The bubble point method is a simple and rapid technique for evaluating effective pore radius of porous media. However, the method is generally only useful for evaluating the larger pore radius of the porous media and is not able to show the pore size distribution of porous media.

The mercury intrusion porosimetry method is more complex than the bubble point method. However, the pore size distributions of porous media can be measured thoroughly by the mercury intrusion porosimetry method. Therefore, the mercury intrusion porosimetry was used to determine the pore size distribution of a wick in this study. For further details of the method, see [13].

2.9 Measurement of porosity

Porosity is the ratio of the volume of the pore space to the total bulk volume in a wick structure. The pore space determines the amount of space available for storage of fluids. The porosity is affected by the average particle size distribution, with a tighter particle size distribution tending towards higher porosities. Higher porosity, which means more and more pores are found in the wick, would make the working fluid flow toward the evaporator more easily and hence increase the heat transfer capacity.

In general, the total porosity can also be divided into effective porosity and ineffective porosity. Ineffective pores represent closed pores which are not interconnected between pore and pore. Effective pores represent interconnected pores which are able to provide pathways for the working fluid. The porosity of a porous structure can be measured by the Arquimedes method according to the ASTM B328-73.

2.10 Measurement of permeability

Permeability indicates the capability of a given porous medium to allow the passage of a fluid and depends on the size of and the degree of connection among the pores of a porous medium. It is another key factor among the wick parameters. Therefore, the higher the permeability, the lower the flow frictions and the pressure drop. The permeability of a porous structure can be determined according to the ASTM E128-61.

In this test, the permeability of a wick sample can be determined by measuring the mass flow rate through the wick for a given pressure drop across the wick. Using Darcy's law for flow through porous media, the permeability can be found as follows:

$$K_{\mathrm{w}} = \frac{\dot{m}\mu_{\mathrm{l}}}{2\pi\rho_{\mathrm{l}}\Delta P L_{\mathrm{w}}} \ln\left(\frac{D_{\mathrm{o}}}{D_{\mathrm{i}}}\right) \tag{5}$$

Here, the uncertainty analysis of permeability was estimated to be within ±4.88%.

3 Results and discussion

To investigate the effects of different biporous wick parameters on a LHP, a 2^3 factorial design was carried out. The experimental data were analyzed by statistical methods. Then, the results were used to confirm the magnitude of these effects and find a direction of potential improvement. Finally, the relationship between the pore size distribution and heat transfer capacity of the wick was discussed.

3.1 Response surface analysis of heat transfer capability for biporous wicks

The results are summarized in Table 3. The significant factors can be determined by the statistical software (DESIGN-EXPERT) to develop a regression model. Then, the response surface plot can be generated by the regression model, which has been discussed extensively in [14]. To reserve the significant factors in the final model, all factors should be scrutinized by hypothesis testing (some prefer significance testing). When the *P*-value of a factor is located under a specified significant level of 0.05, the null hypothesis test will be rejected. In other words, the factor indicates a significant effect at a confidence level of 95%; consequently, the insignificant factor at a significant level of 0.05 is eliminated.

Table 4 summarizes the effect estimates and sums of squares. The largest effects are for particle size of pore former ($A = 44.30$), pore former content ($B = -53.80$),

Table 4 Effect estimate

Factor	Effect estimate	Sum of squares	Percent contribution
A: particle size of pore former	44.30	3,924.98	35.50
B: pore former content	−53.80	5,788.88	52.36
C: sintering Temperature	−21.55	928.81	8.40
AB	−13.80	380.88	3.44
AC	−2.65	14.04	0.13
BC	3.05	18.61	0.17
ABC	−0.15	0.045	4.07×10^{-4}
Cor total		11,056.24	

Table 5 Analysis of variance

Source		Coefficient estimates	Sum of squares	Degrees of freedom	Mean square	F_0	*P*-value
Model			11,023.55	4	2,755.89	252.87	0.0004
Intercept		450.30					
	A	22.15	3,924.98	1	3,924.98	360.14	0.0003
	B	−26.90	5,788.88	1	5,788.88	531.17	0.0002
	C	−10.78	928.81	1	928.81	85.22	0.0027
	AB	−6.90	380.88	1	380.88	34.95	0.0097
Residual			32.70	3	10.90		
Cor total			11,056.24	7			
R^2	0.9970						
R^2_{Adj}	0.9931						
R^2_{Pred}	0.9790						

sintering temperature ($C = -21.55$), and particle size-content of pore former (AB $= -13.80$), although the interaction effect does not appear to have as large an impact on the aggregate value of evaporator temperature as the main effects. The column labeled "percent contribution" measures the percentage contribution of each model term to the total sum of squares. The percent contribution is often a rough but effective guide to the relative importance of each model term. It is noteworthy that the main effects of *A*, *B*, *C* and the AB interaction really dominate this process, accounting for over 99% of the total variability, whereas the AC, BC, and ABC interactions account for less than 1%.

The analysis of variance in Table 5 may be used to confirm the magnitude of these effects. The main effects of *A*, *B*, *C*, and the AB interaction are highly significant (all have very small *P*-values); thus *A*, *B*, *C*, and AB can be taken as significant factors at a confidence level of 95%.

It is noteworthy that the A variable has only a positive effect; that is, increasing the variable raises the aggregate value of evaporator temperature and decreases the heat transfer capacity of biporous wicks. The other *B*, *C*, and AB variables have negative effects; that is, increasing the variables lower the aggregate value of evaporator temperature and increase the heat transfer capacity of biporous wicks.

The following Eq. (6) is the regression model for predicting the aggregate value of evaporator temperature. It can be used to generate response surface plots. Because *R*-squared is quite close to one ($R^2 = 0.9970$), this indicates that the model would be expected to explain the experimental data very well.

$$\begin{aligned}\text{The aggregate values of evaporator temperature} &= 450.30 + 22.15A_{\text{code}} - 26.90B_{\text{code}} - 10.78C_{\text{code}} \\ &\quad - 6.90A_{\text{code}}B_{\text{code}} \end{aligned} \tag{6}$$

Figure 6 presents the response surface and contour plot for the aggregate value of evaporator temperature obtained from the regression model, assuming that sintering temperature is at the high level ($C = 750$°C). The contour plot shows that a direction orientation is dominated by decreasing *A* and increasing *B*, the aggregate value of evaporator temperature will be lower. This probably indicates that increasing *B* can contain more vapors, possess a higher permeability, and improve the probability of large interconnecting pores forming vapor transport channels in biporous wicks. In addition, reducing A can generate more number of large pores to get more vapor transport channels and the evaporating menisci area in the same pore former content.

In view of the preceding analysis, the better heat transfer capacity of the biporous wick shown in Sample 7 appears to be obtained when *A* is at the low level and *B*, *C*, and AB are at the high level, in particular of pore former content (percent contribution $B = 52.36\%$) and particle size of pore former (percent contribution $A = 35.51\%$). This information provides a direction of the potential improvement.

3.2 Effect of the pore size distributions of monoporous wicks on the heat transfer performance

The property of the monoporous wick (Samples 9, 10) was adopted an effective pore radius of 0.7–10 μm and a

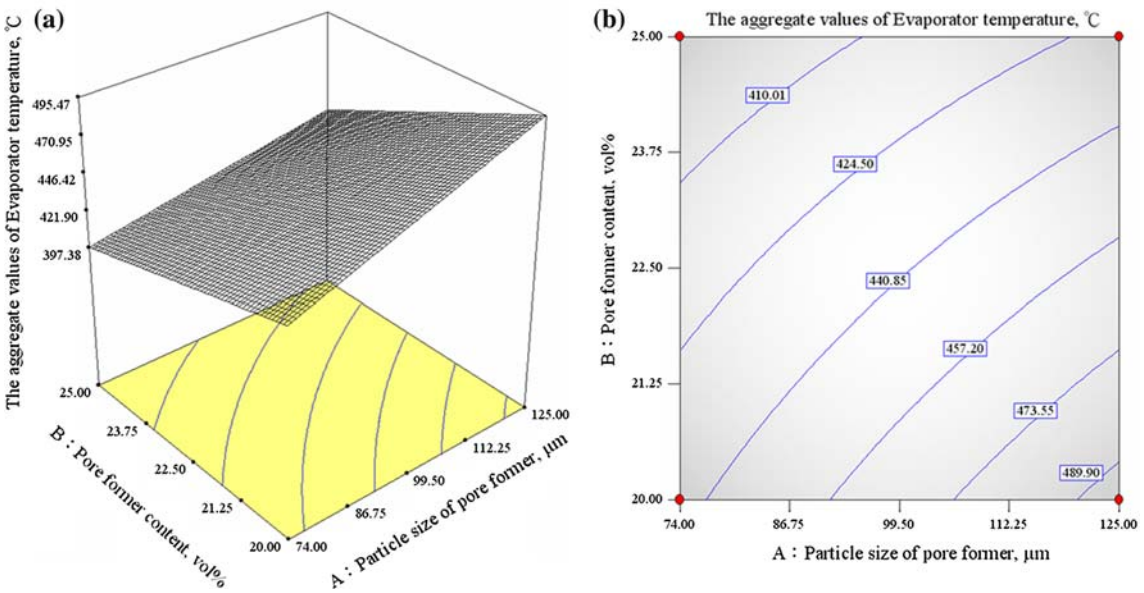

Fig. 6 Response surfaces and contour plot of the aggregate value of evaporator temperature with sintering temperature at the high level ($C = 750$°C) **a** response surface, **b** contour plot

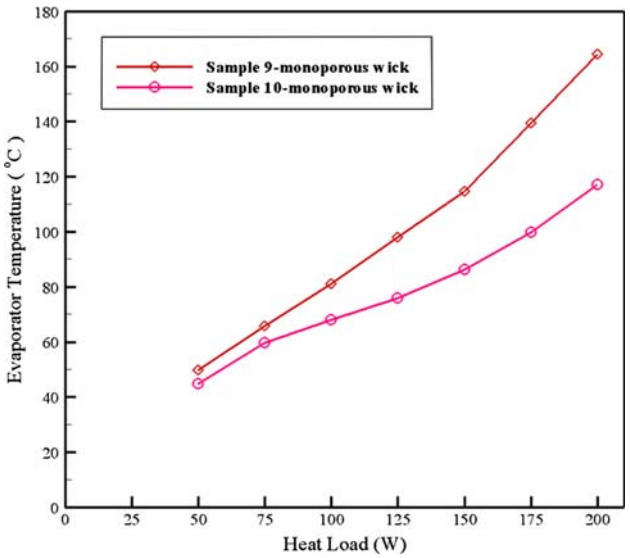

Fig. 7 Evaporator temperature of monoporous wicks at different heat load

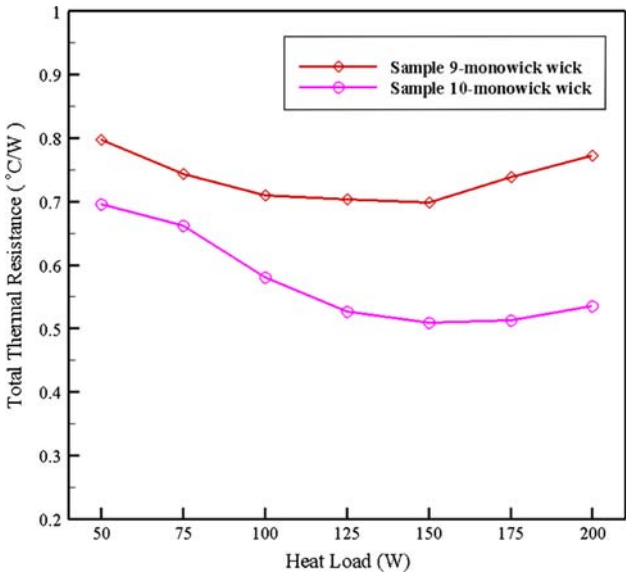

Fig. 9 Total thermal resistance of monoporous wicks at different heat load

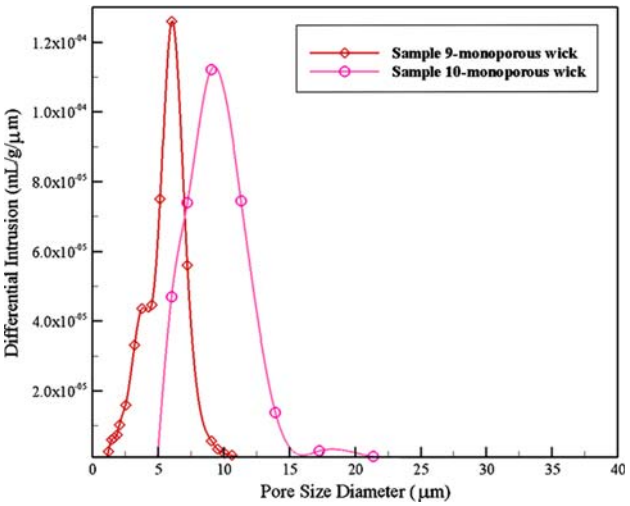

Fig. 8 Measured pore size distributions of monoporous wicks

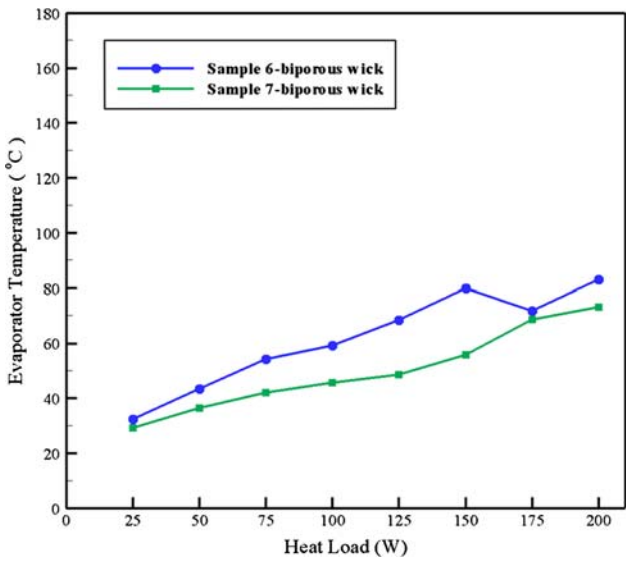

Fig. 10 Evaporator temperature of biporous wicks at different heat load

porosity of 60–75% [15]. The temperature change in the evaporator body was measured by per 25 W and the heat load was increased from 25 to 200 W. Figure 7 shows that, at the sink temperature of 10°C and the allowable evaporator temperature of 80°C, the heat transfer capacity of Sample 10 could achieve 125 W comparing to Sample 9 for 100 W. Sample 10 sintered at 600°C is differentiated from Sample 9 sintered at 700°C by the pore size distribution.

Figure 8 presents that the capillary pressure of Sample 9 with a narrower pore size distribution is higher than that of Sample 10. However, Sample 10 can reach higher heat transfer capacity than that of Sample 9 from Fig. 7. This is because the permeability of Sample 10 could achieve 1.42×10^{-12} m^2 comparing to that of Sample 9 for 9.0×10^{-13} m^2. More specifically, a wider pore size distribution may result in an increased permeability to bear boiling in the wick and alleviate the local dry-out. The total thermal resistance of Sample 10 rises more slowly than that of Sample 9 in Fig. 9. When heat load applied to Samples 9 and 10 exceed 150 W, vapor would accumulate gradually to form the bubbles between the wick and wall. The bubble growth could block the working fluid returning and result in local dry-out. The local dry-out may spread to the whole heating surface with the accumulation of the bubbles. This

not only reduces the heat transfer coefficient but also increases the thermal resistance.

An ideal wick should have small effective pore radius and high permeability. However, these properties are contradictory in the design of a monoporous wick. Therefore, in a design choice, the permeability must be enhanced as far as possible in monoporous wicks after reaching sufficient capillary pressure for a LHP.

3.3 Effect of the bimodal pore size distributions of biporous wicks on the heat transfer performance

As shown in Fig. 10, Sample 7 performs significantly better than Sample 6. This reason could be illustrated in Fig. 11. This is because large pores of Sample 7 are obviously more than those of Sample 6. The permeability of Sample 7 can achieve 10.34×10^{-12} m^2 comparing to that of Sample 6 for 3.86×10^{-12} m^2.

The preceding research results could be explained by the liquid-vapor interface in the wick. The evaporating menisci in a biporous wick include two parts: inverted menisci in small and big pores. When higher heat load is applied to the biporous wick, the inverted menisci in big pores will recede gradually to generate vapor pathways. This not only makes the vapor easily escape from the wick but also enhances the evaporating menisci area in small pores.

Although the permeability of Samples 4 and 8 reflected in Table 3 is higher than that of Sample 7, the heat transfer capacities of Samples 4 and 8 are not better than that of Sample 7. The results indicate that the heat transfer capacity of a biporous wick is not completely determined by the permeability. There exists an optimal ratio between the number and size of large and small pores.

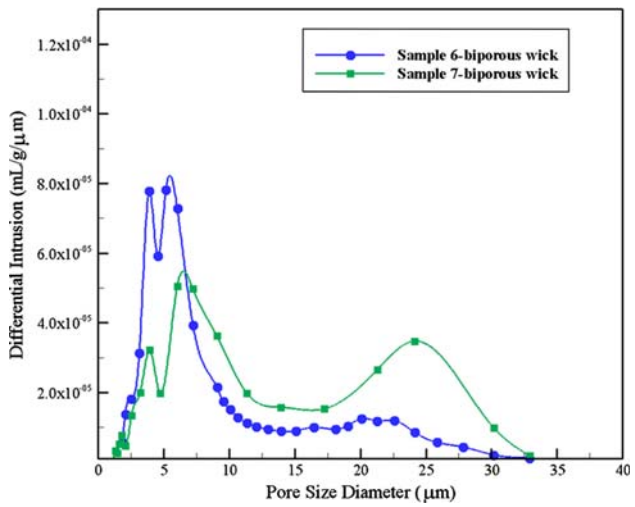

Fig. 11 Measured bimodal pore size distributions of biporous wicks

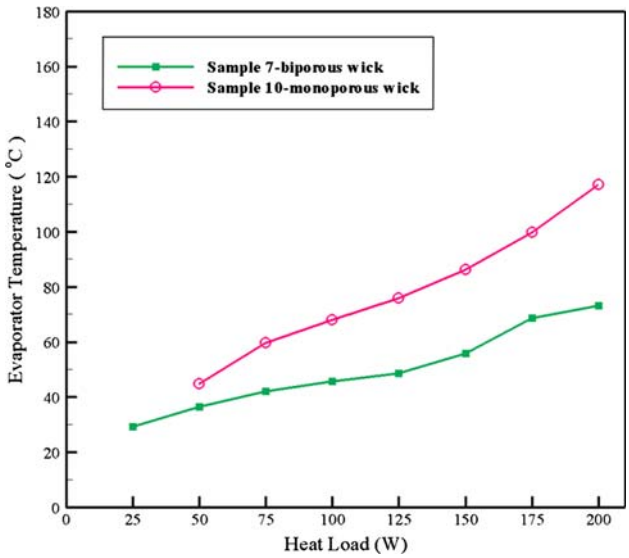

Fig. 12 Evaporator temperature of monoporous and biporous wicks at different heat load

3.4 Comparison of monoporous wicks and biporous wicks

As observed in Fig. 12, the biporous wick (Sample 7) has better heat transfer capacity than the monoporous wick (Sample 10). In addition, Fig. 13 can also provide a better understanding of the difference in pore size distributions between Samples 7 and 10. Sample 7 has obviously two principal pore size distribution regions (mean pore size value $D_1 \approx 7$ μm and $D_2 \approx 24$ μm). Larger pore size distribution (mean pore size value D_2) will lead to an increase in the effective permeability and extend the evaporating menisci area in small pores; smaller pore size

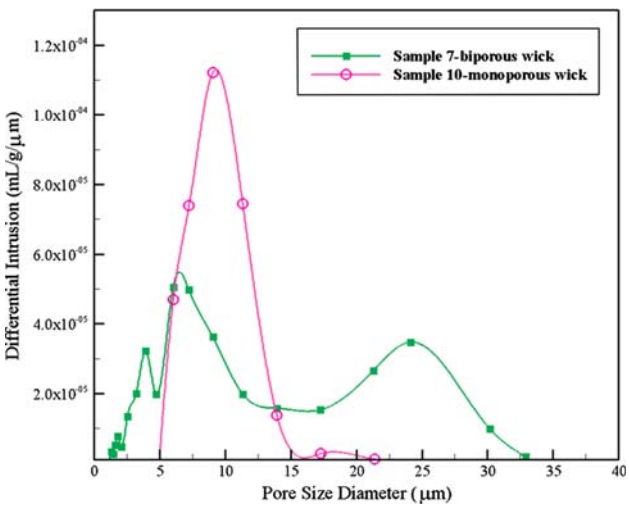

Fig. 13 Measured pore size distributions of monoporous and biporous wicks

distribution (mean pore size value D_1) will improve the heat transfer coefficient. Therefore, the permeability of Sample 7 can achieve 10.34×10^{-12} m^2 comparing to that of Sample 10 for 1.42×10^{-12} m^2. At the sink 10°C and the allowable evaporator temperature 80°C, the heat transfer performance of Sample 7 can reach 200 W. In contrast, Sample 10 can only reach 125 W.

According to the experimental results, the pore size distribution can affect evidently the heat transfer capacity of a wick because the properties of a wick are determined by the pore size distribution before testing. A wick which has the suitable pore size distribution can effectively improve heat transfer coefficient and the evaporative menisci surface area. Therefore, controlling the pore size distribution in a wick will be important.

4 Conclusions

In this study, the heat transfer performance of a biporous wick was enhanced successfully. The study was conducted following a statistical method to analyze the heat transfer capacity of the biporous wicks and to find out the better bimodal pore size distribution for a biporous wick. The major results are listed below:

1. In view of the preceding statistical analysis, the better parameters of the biporous wick seem to tend to more pore former contents (25% by volume), smaller particle size of pore former (74–88 μm), and higher sintering temperature (750°C), in particular of pore former content (percent contribution $B = 52.36\%$) and particle size of pore former (percent contribution $A = 35.51\%$). This information provides a direction of the potential improvement.
2. According to the comparison of the pore size distribution and the statistical analysis, several findings are of interest. First, smaller particle size of pore former (74–88 μm) represented that the evaporating menisci area can be increased in the same pore former content. Second, more pore former content (25% by volume) meant that more vapor pathways can be generated. Third, higher sintering temperature (750°C) indicated that the pore size in a biporous wick will become smaller than before.
3. When the particle size of pore former is 74–88 μm and the pore former content is 25% by volume at sintering temperature 750°C, the large/small pore diameter and permeability of the better biporous wick can be measured as about 24/7 μm and 10.34×10^{-12} m^2. At the sink 10°C and the allowable evaporator temperature 80°C, the heat transfer capacity of the better biporous wick achieved 200 W and the total thermal resistance was 0.31°C/W. Comparing to a monoporous wick for 125 W and 0.53°C/W, the performance is enhanced about 60%. LHPs with biporous wicks are very attractive for high heat flux applications in the future.

References

1. Maidanik YF, Vershinin S, Kholodov V, Dolgirev J (1985) Heat transfer apparatus. US Patent, No.4515209
2. Wolf DA, Ernst DM, and Phillips AL (1994) Loop heat pipes-their performance and potential. SAE Tech Pap Ser (941575)
3. Gerhart C, Gluck D, Stanley S (1999) Initial characterization results of metal wick capillary pumps. In: Space technology and applications international forum, pp 938–942
4. Konev SV, Polasek F, Horvat L (1987) Investigation of boiling in capillary structures. Heat Transfer Sov Res 19(1):14–17
5. Rasor NS, Desplat JL (1989) K-Max: a material with exceptional heat transfer properties. In: Proc intersoc energy convers eng conf, vol 6, pp 2847–2852
6. Rosenfeld JH, North MT (1995) Porous media heat exchangers for cooling of high-power optical components. Opt Eng 34(2):335–341
7. North MT, Saraff DB, Rosenfeld JH, Maidanik YF, Vershinin S (1997) High heat flux loop heat pipes. In: Proc. 6th European symposium on space environmental control systems, Noordwijk, The Netherlands, pp 371–376
8. Chen ZQ, Cheng P, Zhao TS (2000) An experimental study of two phase flow and boiling heat transfer in bi-dispersed porous channels. Int Commun Heat Mass 27(3):293–302
9. Cao XL, Cheng P, Zhao TS (2002) Experimental study of evaporative heat transfer in sintered copper bidispersed wick structures. J Thermophys Heat Transf 16(4):547–552
10. Wang J, Catton I (2001) Biporous heat pipes for high power electronic device cooling. Annu IEEE Semicond Therm Meas Manage Symp, pp 211–218
11. Semenic T, Catton I (2006) Boiling and capillary limit enhancement of a heat pipe wick using biporous wick capillary structure. Annals of the assembly for international heat transfer conference vol 13, PRT-18 p
12. Wang J, Catton I (2001) Evaporation heat transfer in thin biporous media. Heat Mass Transf 37(2–3):275–281
13. Webb PA, Orr C (1997) Analytical methods in fine particle technology, micromeritics instrument corp, Norcross
14. Montgomery DC (2000) Design and analysis of experiments, 5th edn. Wiley, London
15. Maidanik YF (2005) Loop heat pipes-review. Appl Therm Eng 25:635–657